Effect of solution chemistry on the iodine release from iodoapatite in aqueous environments

Zelong Zhang [†][*], Léa Gustin[‡][1], Weiwei Xie[‡], Jie Lian[§], Kalliat T. Valsaraj[‖], and Jianwei Wang[†][⊥]

[†] Department of Geology and Geophysics, Louisiana State University, Baton Rouge, Louisiana 70803 United States

[‡] Department of Chemistry, Louisiana State University, Baton Rouge, Louisiana 70803 United States

[§] Department of Mechanical, Aerospace, and Nuclear Engineering, Rensselaer Polytechnic Institute, 110 Eighth Street, Troy, New York 12180, United States

[‖] Cain Department of Chemical Engineering, Louisiana State University, Baton Rouge, Louisiana 70803 United States

[⊥] Center for Computation and Technology, Louisiana State University, Baton Rouge, Louisiana 70803, United States

*Corresponding to zelongz@lsu.edu

---

[1] Current address: Department of Chemistry, University of Wisconsin-Madison, Madison, Wisconsin 53706, United States

Abstract

To ensure the safe disposal of nuclear waste, understanding the release process of radionuclides retained in the nuclear waste forms is of vital importance. Iodoapatite $Pb_{9.85}(VO_4)_6I_{1.7}$, a potential waste form for iodine-129, was selected as a model system for ceramic waste forms in this study to understand the effect of aqueous species on iodine release. Semi-dynamic leaching tests were conducted on bulk samples in cap-sealed Teflon vessels with 0.1 mol/L $NaCl$, Na_2CO_3, Na_3PO_4, and Na_2SO_4 solutions under 90 °C, fixed sample surface area to solution volume ratio of 5/m, and periodic replacement of leaching solutions. The reacted solutions were then analyzed by Inductively Coupled Plasma-Mass Spectrometry and Inductively Coupled Plasma-Optical Emission Spectrometry; the leached surfaces were characterized by X-ray diffraction, scanning electron microscopy, and infrared spectroscopy. The result shows that, compared to deionized water, the ion-rich solutions enhanced the iodine release as a result of the increased ionic strength, reduced activity coefficient of dissolved species, and increased solution pH. Surface reactions can lead to the formations of secondary phases by ion-exchange and precipitation of secondary phases. These findings suggest that an ion-rich environment in the geological repository can be detrimental to the disposal safety of the apatite waste form.

Broader context

Nuclear power is a low emission energy that can mitigate climate change. However, nuclear power plants produce radioactive waste which requires safe disposal to minimize its risk to biosphere. Due to the long half-life of several waste radionuclides (e.g. iodine-129: 15.7 million years), it is imperative to ensure the long-term integrity of the nuclear waste forms to prevent the release of radionuclides in disposal environments. Since the most probably scenario for waste forms to be compromised is exposing to an aqueous environment, we conducted leaching experiments to characterize the iodine release mechanism from bulk samples of iodoapatite, a promising waste form for iodine, in different aqueous solutions to imitate natural settings. To date, this is the first study to systematically characterize iodine release mechanisms from a nuclear waste form in aqueous environments. The findings of this study provide a theoretical framework for improving long-term disposal safety of nuclear waste.

Introduction

Nuclear power supplies low-carbon energy. Nuclear power supplies low-carbon energy. The deployment of nuclear energy is motivated by the pressing demand to mitigate climate change.[1] Sustainable development of the nuclear energy requires concrete plans to safely dispose radionuclides waste generated by nuclear fission.[2] Among those radionuclides, iodine-129 is particularly challenging to handle due to its long half-life (15.7 million years), high yield (0.7% yield per fission of uranium-235),[3] and weak interactions with common materials in repository environments such as engineering barrier and rock in geology formation.[4,5] Iodide (I^-) is the most stable form of iodine in an environment with pH and redox potential typically found in nature.[6–8] Under highly oxidizing conditions, iodide can be oxidized to iodine (I_2) and/or iodate (IO_3^-). All these iodine species are highly mobile in nature given their high volatility and or high solubility.[9,10] Iodine, as an essential element for human health, can accumulate in human bodies.[11] For a healthy adult, 30% of the total iodine, approximately 15-20 mg, is concentrated in the thyroid gland.[12] Chronical radiation from iodine-129 beta decay can induce cancer to the thyroid follicular cells.[11] Therefore, the iodine-129 is a primary contributor of the radiation dosage when analyzing the safety of disposal environments.[4] The immobilization of iodine-129 is one of the critical research subjects for nuclear waste management.[4,13–18]

The most probable scenarios that compromise nuclear waste forms in a repository environment are the contact with aqueous solutions.[19,20] In a typical repository, nuclear waste forms are packed into corrosion resistant metallic canisters underground.[21] Canister corrosion and degradation are anticipated to be the result of corrodents carried by groundwater.[22] Through infiltration and percolation of precipitation and groundwater aquifer, water can reach the canisters and supply corrodents to react with the canister material. Upon the breaching of the

canister, the waste forms are exposed to an aqueous environment. Owing to the long half-life of iodine-129, it is crucial to predict the long-term chemical durability of iodine waste forms. To enable such prediction, it is necessary to obtain a fundamental understanding of corrosion mechanisms of waste forms and how iodine in the host material is released in various solutions that may occur under repository conditions.

Several waste form materials including glass, ceramics, glass-ceramics, cement, and composite have been proposed to immobilize iodine.[18,23] These waste forms immobilize iodine via two major mechanisms: encapsulation and incorporation. To encapsulate iodine, the host matrices need to contain iodine in a designated phase different from the host material. One example is AgI, an iodine-bearing phase encapsulated by aluminophosphate glass matrix.[24] Iodine can also be incorporated as a compositional element into the host matrix structure through chemical bonding, such as iodoapatite $Pb_5(VO_4)_3I$ and sodalite $Na_4(AlSiO_4)_3I$.[13,25–27]

The difficulty to study the durability of different waste forms varies on a case-by-case basis. It is particularly challenging to evaluate the encapsulation waste forms due to the complexity of multi-phase and microstructures. On the other hand, characterizing the corrosion mechanism can be relatively straightforward for single-phase crystal waste forms which have well-defined crystal structures and simple microstructures. Based on the simplicity of its crystal structure and microstructure, iodoapatite is chosen in this study as the model system of ceramic waste forms that can incorporate radionuclides. In addition, apatite ceramics is a promising material due to its thermal, mechanical, and chemical stability.[13,25,28,29] These advantages are also demonstrated in nature as apatite has been found as a retention matrix for actinides and fission products in natural fission reactors at Franceville basin in Africa.[22,30]

Several chemical durability tests have been performed on single-phase crystal waste forms. Uno et al. in 2001 conducted soxhlet leach method on apatite $Pb_{10}(VO_4)_6I_2$.[31] Soxhlet leach method is designed to maximize the number of leachable constituents in leachant by allowing a continuous contact between the waste and recycling leachant in a closed system.[32] The iodine release rate, 3.98×10^{-5} g·cm^{-2}·d^{-1}, was reported.[31] Guy et al. in 2002 studied apatite $Pb_{10}(VO_4)_{4.8}(PO_4)_{1.2}I_2$ dissolution in aqueous solutions.[33] The resulting data shows that iodine release was incongruent and exhibited dependency on temperature and pH. They also discovered a secondary phase, lead vanado-phosphate, precipitated at the sample surface. Zhang et al. in 2007 performed static leaching test on $Pb_5(VO_4)_3I$ powder in a basic KOH/KHCO$_3$ buffer solution.[34] Spectroscopic evidences show that OH$^-$ and CO$_3^{2-}$ can substitute I$^-$ and VO$_4^{3-}$ in apatite. Maddrell et al. in 2014 conducted static leach tests on crushed powder iodide sodalite $Na_4(AlSiO_4)_3I$ in KOH/KHCO$_3$ buffer solutions.[26] The result suggests a congruent dissolution.[26] Three leaching static experiments with durations of 3, 7, and 14 days exhibited a logarithmic increase of iodine release. More recently, in 2017 Coulon et al. applied static leaching technique to study the iodate-substituted hydroxyapatite in deionized water and groundwater.[35] They reported that the iodine release is controlled by congruent dissolution under unsaturated conditions and controlled by diffusion through ion exchange under saturated condition. Interestingly, when groundwater was used as leachant, secondary phase hydroxyapatite precipitated on the sample surface. Based on these studies, static leach test is a preferable method to study the waste form durability due to the following reasons: 1) its simple procedure can accommodate a wide range of test conditions; 2) the resultant data can be used to interpret the release mechanism.[36] Static leaching method assumes that the solution feedback is negligible, which is valid under conditions of sufficiently low surface to volume ratio.[36] However, the

solution feedback can gradually increase over time in a static leaching experiment. In cases where the solution is oversaturated for phases of low solubility, secondary phases can precipitate at the leached surface. Therefore, it can be problematic to use data from static leaching tests to predict waste form behavior in a repository environment.[37] To address the issues of solution feedback, a semi-dynamic leaching method was implemented by Zhang et al. in 2018 to quantify the processes involved in the iodine release of an iodine-bearing apatite.[29] In their experiment, deionized water solutions, as the leachant, were replaced periodically to minimize the solution feedback. They demonstrated that iodine released from apatite is driven by short-term diffusion and long-term matrix dissolution. This semi-dynamic approach was employed to produce essential datasets to parameterize a mechanistic model suitable for predicting the kinetics of iodine release under different conditions.[37]

Since the aqueous systems in natural environment contain a variety of dissolved species, it is necessary to understand how these aqueous species affect the iodine release from iodine waste forms in an aqueous environment. For instance, the iodine release from apatite structured materials can be enhanced by rapid substitution of halogen element[38–41] or inhibited by precipitation of secondary phase.[33,35,37] In this study, we conducted semi-dynamic leach tests on single phase crystal ceramics of iodoapatite in 0.1 mol/L NaCl, Na_2CO_3, Na_3PO_4 and Na_2SO_4 solutions. The goal is to examine the impact of the solution chemistry on the kinetics of iodoapatite dissolution. We hypothesized that dissolved aqueous species, via ion exchange and precipitation, can substantially impact the dissolution kinetics; this effect should highly depend on the chemistry of the aqueous species and the surface reactions of specific phases. The finding of this study is expected to provide important insight into the long-term performance of iodine waste forms and guidance to improve the disposal safety of nuclear waste.

Experimental

Materials and methods

The samples, obtained from previous studies,[25] were dense ceramic chips in quadrilateral shape: 4.7 – 10.3 millimeter long by 1.1 – 1.8 millimeter thick with a chemical composition of $Pb_{9.85}(VO_4)_6I_{1.7}$ according to the EDS and X-ray diffraction refinement, as shown in Figures 1, 2 and 4. The iodoapatite samples were synthesized by using high energy ball milling (HEBM) and spark plasma sintering (SPS) techniques. Sample surfaces were polished by 4000-grit sandpaper on a mechanical polishing wheel lubricated with ethanol. Details of the synthesis and characterization of these samples were reported previously in separate publications.[25,29,37]

The leaching method was adopted from ASTM C1308 standard test, as described in the previous study[29,37]. Four parallel experiments were conducted simultaneously for 14 days in four different leaching solutions: 0.1 mol/L NaCl, 0.1 mol/L Na_2CO_3, 0.1 mol/L Na_3PO_4, and 0.1 mol/L Na_2SO_4. Sample surface area (m^2) to solution volume (m^3) ratios (S/V) of all four tests were fixed and maintained at 5/m. The leached solutions were replaced every 24 hours. All reactor vessels were weighed before and after each interval to monitor the solution losses which were within 0.5 % of the initial solution mass. In addition, a control test was conducted in deionized water under identical conditions for 7 days using the same protocol. All samples after leaching experiments were collected, rinsed by deionized water and ethanol, and air-dried.

Characterization

The elements of interest in the leachate solutions are I, Pb, and V. The leached solutions, depending on the solution chemistry, were analyzed by Inductively Coupled Plasma-Mass Spectrometry (ICP-MS, PerkinElmer Elan 9000) and/or Inductively-Coupled Plasma-Optical Emission Spectrometry (ICP-OES, SPECTRO Ametek Spectro ARCOS). Two standard solutions from Inorganic Ventures were used in the solution analysis: 1) 1.001 ± 0.007 µg/ mL iodide in H_2O solution and 2) 1.000 ± 0.007 µg/ mL lead and 1.000 ± 0.006 µg/ mL vanadium in 1% HNO_3 solution. Solution chemistry at equilibrium state such as pH, ionic strength, speciation, and activity were calculated by Visual MINTEQ package.

Samples were characterized by Scanning Electron Microscopy (SEM), Infrared spectroscopy (IR), and X-ray diffraction spectroscopy (XRD). SEM images were taken by a FEI Quanta SEM system with FEI Versa 3D DualBeam. Infrared spectroscopy was performed on a Thermo Nicolet Continuum Infrared Microscope under Specular Reflection mode and transmission mode with a fixed incident angle and an aperture area of 10 by 10 µm covering 4000 to 650 cm^{-1} at a spectral resolution of 2 cm^{-1}. XRD data were collected from PANalytical Empyrean X-Ray Diffractometer equipped with monochromated Cu-Kα radiation ($\lambda = 1.5406$ Å), operated at 45 kV, 40 mA, a step size of 0.026°, and a scanning range from 5 to 100°.

The crystal structures were refined by Le Bail algorithm using Jana2006 program.[42] All parameters were refined by the least-squares method. The pseudo-Voigt function was used as the peak profile function. Structural parameters of $Pb_{9.85}(VO_4)_6I_{1.7}$ measured by Audubert et al. were used as initial input (hexagonal, space group P63/m, a = b = 10.422 Å, c = 7.467 Å, $\alpha = \beta = 90°$; $\gamma = 120°$).[43]

Results

Leached surface characterization by SEM/EDS

In Figure 1 (a-c), no changes observable by naked eyes occurred on the surfaces of samples leached by NaCl and NaSO$_4$ solutions for 14 days, whereas white layers were gradually formed on the sample surfaces leached by Na$_2$CO$_3$ and Na$_3$PO$_4$ solutions within the first week of the experiments. The SEM images in Figure 1 (d-i) show that the surface alterations on samples leached by NaCl and Na$_2$SO$_4$ solutions were moderate, similar to the water leached surface. However, samples leached by Na$_2$CO$_3$ and Na$_3$PO$_4$ solutions demonstrated significant surface corrosion and possible formation of new phases. The surface leached by Na$_2$CO$_3$ exhibited large grains, while congregated structures of similar size appeared on the surface leached by Na$_3$PO$_4$.

According to EDS analysis, the surface chemical compositions in Figure 2 indicate considerable changes between the leached samples and the pristine one. The key features of EDS spectrum of pristine iodoapatite are: a carbon peak at 0.3 keV from background (carbon tape), an oxygen peak at 0.5 keV, a broad Pb band from 2.34 to 2.45 keV shouldered with two small Pb peaks at 1.8 and 2.6 keV, three iodine peaks at 3.9, 4.2, and 4.5 keV, and vanadium peaks at 4.9 and 5.4 keV. Overall, the iodine peaks at 3.94 keV are nearly diminished in the EDS spectra of all four leached surfaces. The samples leached by NaCl and Na$_3$PO$_4$ exhibited a substantial amount of chloride and phosphorus signals at 2.62 and 2.01 keV, respectively. On the sample leached by NaCl, the Pb peak at 2.62 keV is comparable to the Pb peak at 1.8 keV, while the 2.62 keV peaks of the rest samples are much weaker than their corresponding 1.8 keV peaks. Carbon signal at 0.27

keV from Na_2CO_3 leached sample cannot be properly quantified due to the background interference from carbon tape and the graphite impurity introduced during sample synthesis. Sulfur EDS peak at 2.31 keV overlaps with the broad central peak of Pb at 2.34 keV. Na_2SO_4 leached surface exhibited no sulfur peak near 2.3 keV given the resemblance of the band shape between the sample leached by Na_2SO_4 and the rest. We noticed variations of carbon and oxygen EDS signals among these samples which were induced by the instrumentation settings such as sample orientation and beam parameters. Therefore, carbon and oxygen were not considered in the EDS analysis.

Leached surface characterization by IR analysis

The IR spectroscopy results are listed in Figure 3. All these four samples yielded two main peaks near 750 and 890 cm^{-1}, which are attributed to V-O bond.[34] Pristine iodoapatite and samples leached by water, Na_2SO_4, and NaCl showed nearly identical spectra. Surfaces leached by Na_2CO_3 and Na_3PO_4 exhibited position shifts of these two V-O peaks to the region of 700 to 900 cm^{-1} and multiple new bands. Sample leached by Na_2CO_3 yielded sharp bands near 785, 890, 960, 1200, and 1450 cm^{-1}, in which the broad band at 1450 cm^{-1} is attributed to the stretching vibration of CO_3^{2-}.[44,45] The Na_3PO_4 leached surface generated IR peaks near 785, 870, 950, 1110, 1420, 1800, and 2200 cm^{-1}, in which some can be assigned to the PO_4^{3-} (e.g. $v_1 - 950$ cm^{-1}, $v_3 - 1100$ cm^{-1}).[44] Interestingly, both CO_3^{2-} and PO_4^{3-} leached surfaces showed visible OH$^-$ stretching vibration near 3500 cm^{-1},[34,44] which also occurred on water leached surface under IR transmission mode.[29]

Leached surface characterization by XRD

The XRD data are shown in Figure 4. All these leached samples demonstrated substantial differences compared to the pristine sample. Based on the XRD pattern, these leached samples can be categorized into two groups: I) surfaces leached by NaCl and Na_2SO_4 solutions, the pristine, and water leached sample; II) surfaces leached by Na_2CO_3 and Na_3PO_4 solutions, which were similar to the standard hydroxylvanadinite. The XRD patterns of Group I are alike, which indicates no substantial structural changes compared to the pristine. The XRD patterns of Group II display enhanced peak splitting between 25° and 28°. The original peak splitting of the pristine sample reflects the apatite structure deformation which accommodates the relatively large iodide incorporated in the apatite framework. The peak splitting of Na_2SO_4 leached surface is slightly enhanced, compared to the pristine, but is weaker than the water leached sample. Interestingly, NaCl leached surface yielded a diminished splitting at 26° and a new peak occurred at 29°, later identified as $1\bar{3}1$ shown in Figure 5. The Full Width at Half Maximum (FWHM) of XRD from NaCl leached surface was considerably broadened to ~0.4° compared to ~0.2° from other samples, which may be attributed to the peak overlapping resulting from the presence of a secondary phase. Both Na_2CO_3 and Na_3PO_4 leached samples exhibited nearly identical XRD pattern, resembling the pattern of standard hydroxylvanadinite $Pb_{10}(VO_4)_6(OH)_2$. The two highest bands on $Pb_{10}(VO_4)_6OH_2$ standard are 112 and $1\bar{3}1$ with an order of intensity $I_{112} < I_{1\bar{3}1}$. Same bands 112 and $1\bar{3}1$ also have the highest intensity on Na_2CO_3 and Na_3PO_4 leached samples, however, the intensity of 112 is higher than that of $1\bar{3}1$, $I_{112} > I_{1\bar{3}1}$.

The Le Bail method was applied to obtain structural information from the XRD data. Table 1 compares the refined lattice parameters between sample surfaces of different

conditions and standards. No noticeable changes occurred in the crystal structures of samples leached by deionized water and Na_2SO_4 when compared to that of pristine sample (their length of a-, b-, and c-axes are approximately ~10.4, ~10.4, and ~7.5 Å, respectively). On the other hand, a ~0.2 Å contraction along both the a- and b-axes were observed for the samples leached by Na_2CO_3 and Na_3PO_4 solutions while the c-axis remains the same and is consistent with other samples at ~7.45 Å. The observed and calculated diffraction patterns, the residual and the indices of the main reflections of NaCl leached sample are shown in Figure 5. We identified a secondary phase vanadinite $Pb_5(VO_4)_3Cl$, indicating the substitution of iodine by chlorine during NaCl leaching.

Solution composition analysis by ICP-MS and ICP-OES

The results of the solution analysis on the leachates collected from the leach tests are shown in Figure 6. The release rates of iodine, lead, and vanadium are depicted as green circles, blue squares, and red triangles, respectively. In Figure 6(a), iodine release in NaCl solution gradually increased over time, reaching a maximum rate near 0.8 mmol/m^2/d at day 11, and then slightly decreased near the end of the 14-day test. The Pb and V release exhibited similar patterns with a relatively high initial rate around 0.075 mmol/m^2/d, then gradually decreased, and eventually approached a plateau near 0.05 mmol/m^2/d. In Figure 6(b), the release patterns of iodine and vanadium in Na_2CO_3 are similar: release rates rapidly reached maximum near day 2 and then gradually decreased over time approaching a plateau. However, the long-term rate of Pb in Na_2CO_3 appears to be constant. In Figure 6 (c), the iodine release in Na_2SO_4 exhibited a high initial rate approximately 0.32 mmol/m^2/d and then its rate gradually decreased, eventually approaching a plateau around 0.15 mmol/m^2/d. Despite no high initial release, the Pb and V release patterns follow the

trend of iodine release: gradually decreased over time and then rebounded near day 10. The Figure 6(d) describes the element release of iodoapatite in Na_3PO_4, which shows constant rates of ~4.5, ~3.5, and ~13 $mmol/m^2/d$ for the release for iodine, Pb, and V, respectively. Due to the instrumentation limitation and sample consumption, only four leachates from the Na_3PO_4 experiment was analyzed for their Pb content.

Leaching rates of I, Pb, and V based on the solutions analysis are compared in Figures 7(a-c), respectively. In general, leaching tests conducted in the ionic solutions present significantly higher element release rates than those of deionized water in the order of $Na_3PO_4 > Na_2CO_3 > Na_2SO_4 >$ water, except in the NaCl solution. In Figure 7(a), iodine release from Na_3PO_4, Na_2CO_3, and Na_2SO_4 solutions exhibited a long-term leach pattern similar to that of water leaching: started with a high initial release, then gradually decreased, and eventually stabilized and reached a plateau. The iodine release in NaCl solution, however, presents a different pattern: iodine rate increased from the beginning of leach test to day 11, when the rate reached maximum and then stabilized. The release rates of Pb and V from NaCl test are relatively constant but not higher than those of water leached as shown in Figures 7(b, c).

The molar ratios in leachate solutions are illustrated in Figures 7 (d, e). Except for the anomalous NaCl data, the long-term I/V ratios in Figure 7(d) fluctuate around the ratio of water-leached sample within the range of [0.34, 1.02], which are higher than the stoichiometric value 0.28. In Figure 7(e), the long-term Pb/V ratios of NaCl and Na_2SO_4 tests are 1.36 and 1.65, approximate to the stoichiometric value 1.64, whereas the long-term ratios from Na_2CO_3 and Na_3PO_4 tests are 0.95 and 0.27, significantly lower than 1.64.

Overview of leaching rates in solutions

The phases of interest in this study are the aqueous solutions and the solid surfaces. The leachate solution chemistry in Figure 7 shows that iodine release from the sample leached by the NaCl solution has a distinctive pattern. For the other leach tests, the long-term iodine rates (plateau region in Figures 6-7) are at least one magnitude higher than that from water leaching. And the order of iodine leach rate, based on solution analysis in Figure 7 (a), is consistent with the orders of Pb and V rates in Figure 7 (b, c): $R_{Pb/V/I}$ $(Na_3PO_4) > R_{Pb/V/I}$ $(Na_2CO_3) > R_{Pb/V/I}(Na_2SO_4) > R_{Pb/V/I}$ (deionized water). In the following section, we will analyze the anomalous result of NaCl leach test and then explain how element release behaviors differentiate due to the different solution chemistry, such as pH and ionic species.

Discussion

Anomaly of the sample leached by NaCl solution

Iodoapatite sample leached by 0.1 mol/L NaCl solution exhibited unique surface phase composition and iodine release pattern. The XRD data in Figures 4 and 5 show leached surface has no apparent splitting in the region from 25° to 28° (2θ) and a new peak ($1\bar{3}1$), attributed by a vanadinite phase. This anomaly suggests a reduced structural distortion, which can be contributed by substituting iodide with smaller chloride. The refinement in Figure 5 confirmed new phase vanadinite was formed on the surface, which resembles the XRD pattern of iodoapatite $Pb_{9.85}(VO_4)_6I_{1.7}$. The XRD data is consistent with the EDS result and solution analysis. The Pb EDS band at 2.6 keV, in Fig 2, is comparatively enhanced due to the overlap by chlorine signal at 2.6 keV. The release

rates of iodine from the NaCl test in Figure 6(a) suggest the new phase was growing until the equilibrium state was reached. A similar iodine release pattern was observed in a pH 4 semi-dynamic leaching experiment, in which the rate anomaly was caused by the formation of a secondary phase.[37] The molar ratios of Pb/V in Figure 7(e) approximate to the stoichiometric value 1.6, indicating a congruent dissolution of Pb and V. The variation of I/V molar ratios in Figure 7(d) is consistent with that of iodine rates in Figure 6(a). Both the I/V ratios and iodine rates suggest an incongruent release for iodine, unlike the congruent Pb and V. The SEM images in Figures 1(b, e) show that both surfaces leached by NaCl and deionized water share similar morphology. The new phase vanadinite $Pb_5(VO_4)Cl$, confirmed by the XRD refinement, suggests ion-exchange process between iodide and chloride. This postulation is supported by the solution and surface analysis that 1) a significant amount of iodine was released into NaCl solution while the Pb and V rates are comparable to the data of water leach test as shown in Figures 6-7; 2) the surface alteration revealed by SEM in Figure 1 and the surface chemistry by EDS in Figure 2 resemble those of deionized water. Interestingly, the structural deformation of the original iodine-bearing apatite $Pb_{9.85}(VO_4)_6I_{1.7}$ appeared to be restored in the chlorine-substituted structure vanadinite $Pb_5(VO4)_3Cl$. Given that the ionic radius of chloride (Cl^-, 1.68 ± 0.19 Å) is considerably smaller than that of iodide (I^-, 2.11 ± 0.19 Å),[46] exchanging the iodide with smaller chloride seems to have repaired the structural deformation.

Effect of pH on iodine release and secondary phase formation

The solution pH has a strong effect on the iodine release of the iodoapatite. Parameters of the solution chemistry calculated by VMINTEQ are listed in Table 2. According to our previous studies, iodoapatite dissolution in deionized water can be represented by the

congruent release of Pb and V.[29] In Figure 7 (b, c), the Pb and V rates from different

solutions are generally constant, indicating a constant-dissolution controlled process. The

overall dissolution rates from low to high appears to be: R *(deionized water)* $< R$

(Na_2SO_4) $< R$ (Na_2CO_3) $< R$ (Na_3PO_4), which corresponds to the solution pH values ~6.1,

~6.2, ~10.3, and ~10.9 under 90 °C as listed in Table 2. Therefore, increasing pH from

neutral to basic can increase the iodine release by enhancing the overall dissolution of the

iodoapatite, which is consistent with previous experimental results on synthetic

iodoapatite and natural apatites[33,47]. However, due to the secondary phase formed in

Na_2CO_3 solutions, the dissolution process was being continuously hindered by the

accumulating precipitates. Interestingly, the trend of iodine released in Na_2CO_3 solution

of pH 10.3 resembles that of leaching iodoapatite under pH 4.[37] Despite the rate

difference, both surfaces leached by pH 4 and pH 10.3 formed secondary phases

(chervetite and hydroxylvanadinite, respectively). Our previous study showed that the

equivalent long-term rate of iodine release under pH 6 is 8.1 mmol/m^2/d, over two

magnitudes higher than that of the deionized water 0.036 mmol/m^2/d.[37] Nevertheless, the

release rates of iodine leached by the solutions of non-neutral pH are at least one

magnitude higher than that of the neutral pH solutions due to the enhanced dissolution

process.

Surface characterizations indicate the presence of new phases under the basic

conditions. The XRD analysis in Figure 4 and Table 1 shows the surfaces leached by the

Na_2CO_3 and Na_3PO_4 solutions were dominated by secondary phases resembling

hydroxylvanadinite $Pb_{10}(VO_4)_6(OH)_2$. The SEM in Figure 1 reveals different grain shapes

and sizes from the water leached, while the EDS in Figure 2 demonstrates that iodine was

depleted on the surface. The solution analysis also supports the formation of new phase given the similar element release pattern to that of pH 4 and incongruent Pb/V ratios far away from the stoichiometric value. As shown in Figure 7, the leaching rates of all elements are at least one magnitude higher than the water leach rates of corresponding elements. The results from this study and those from relevant literature suggest that the solution pH exerts significant effects on the dissolution rate and the secondary phase formation in aqueous environments such as chervetite and hydroxyvanadinite precipitated under acidic and basic conditions, respectively.[37,48,49]

Effect of ionic species on the dissolution rate

In this study, dissolved species affected the sample dissolution process by increasing the ionic strength in solution, which consequently reduced the activity coefficient of dissolved species. As a result, saturation state and solution feedback were reduced, which in return increased the dissolution rate.[47] Although the 0.1 mol/L Na_2SO_4 and 0.1 mol/L NaCl solutions have approximately the same solution pH as deionized water, the dissolution rates in these ionic solutions are significantly higher than that of the deionized water. As shown in Table 2, 0.1 mol/L Na_2SO_4 solution gives total ionic strength of 0.26 mol/L, 0.1 mol/L NaCl solution 0.098 mol/L, and deionized water 2.04×10^{-6} mol/L close to zero. The vast difference in ionic strength leads to different degrees of saturation state. The activity coefficient of the major ions Na^+, Cl^-, and SO_4^{2-} in these ionic solutions are ranging from 0.25 to 0.76, considerably lower than the major ions H^+ and OH^- with a respective activity coefficient 1.00 in the deionized water. The dissolution rate in 0.1 mol/L Na_2SO_4 solution is higher than the rate in the 0.1 mol/L NaCl solution and deionized water under the same pH and reaction mechanism, as shown in Figure 7.

Moreover, the average release rate of iodine in Na_3PO_4 (pH 10.9) is about one magnitude higher that of Na_2CO_3 (pH 10.3) despite their similar pHs. The difference in rates can be inferred from the difference in ionic strength: 0.29 mol/L for 0.1 mol/L Na_3PO_4 and 0.25 mol/L for Na_2CO_3 solution.

In addition, no substantial structure change happened to the sample leached by 0.1 mol/L Na_2SO_4 solution. It is unlikely that anion SO_4^{2-} can be incorporated into apatite structure as there is no evidence from surface characterization and solution analysis to support that. No structural change was detected by the XRD characterization. The SEM images and EDS analysis in Figures 1 and 2 show that the Na_2SO_4 and water leached surfaces have a similar grain size, surface morphology, and chemical composition. The element release rates and ratios in Figure 7 and 8 demonstrate a similar leach behavior between samples leached by Na_2SO_4 and deionized water. The similarities in surface alteration and leaching behavior between samples leached by Na_2SO_4 and water suggest that the iodine release in Na_2SO_4 solution was controlled by short-term diffusion and long-term dissolution and the release of Pb and V is controlled by congruent dissolution. No precipitated was observed on Na_2SO_4 leached surface, which is also similar to the surface leached by water.

In terms of the surface precipitation, the SEM images in Figures 1 (c, f) reflect intense surface alterations in the solutions of Na_3PO_4 and Na_2CO_3. The leached surfaces yielded XRD patterns similar to the standard hydroxyvanadinite $Pb_5(VO_4)_3(OH)$. However, significant contractions of *a*- and *b*-axes as shown in Table 2 indicate the size of VO_4 site was reduced, which could be caused by a substitution of smaller groups.[50] The IR spectroscopy of the sample leached by Na_3PO_4 confirms the existence of P-O bond and

OH$^-$. Furthermore, the EDS detected phosphorus signal, which also supports that PO$_4$ group was in VO$_4$ site. The molar ratios of Pb/V in Figure 7 show a deficiency of Pb relative to V in Na$_3$PO$_4$ leaching test. These evidences suggest the precipitates are a product of hydroxyvanadinite with mixed site: Pb$_{10}$(VO$_4$)$_n$(PO$_4$)6-$_n$(OH)$_2$. The site mixing is possible since Pb$_{10}$(VO$_4$)$_x$(PO$_4$)$_{6-x}$(OH)$_2$ can occur during wet chemistry reactions under similar conditions.[48] Carbonate is known to be incorporated into apatite structure by substitution.[50–53] Given that phosphate (PO$_4^{3-}$, ionic radius 2.30 ± 0.42 Å)[46] can replace vanadate in iodoapatite,[48] it is reasonable to presume that carbonate of a smaller ionic radius (CO$_3^{2-}$, 1.89 ± 0.19 Å)[46] can substitute vanadate in a similar crystal structure. Therefore, the secondary phase formed on in the Na$_2$CO$_3$ solution is Pb$_{10}$(VO$_4$)$_{6-m}$(CO$_3$)$_{1.5m}$(OH)$_2$.

Mechanism of iodoapatite dissolution and surface reactions in aqueous environments

Figure 8 generalizes the mechanism of iodoapatite dissolutions with multiple processes contributing to the iodine release. Our previous study on iodine release in deionized water suggests that the iodine release is driven by short-term diffusion and long-term dissolution.[29] Diffusion and dissolution are affected by various factors of the solution chemistry, such as solution ionic strength, pH, and secondary phase formation resulted from a supersaturation of the solution with respect to low solubility species. In neutral pH solutions, the iodine release is subjected to the substitution of iodine by anionic species in solution such as OH$^-$ and Cl$^-$. When dealing with solutions of comparable pH, a higher ionic strength, due to the ionic content, can enhance the dissolution by changing saturation conditions. Solution pH other than near neutral can

increase the dissolution by exponentially accelerating the dissolution process. The resulting rapid dissolution can often lead to the precipitation of secondary phases when the solution approaches the supersaturation state of low solubility phases. Possible secondary phases include chervetite $Pb_2V_2O_7$ under acidic condition[37] and hydroxylvanadinite $Pb_5(VO_4)_3OH$ under basic condition.

Conclusions

The present study of the effect of solution compositions on iodoapatite dissolution suggests that the higher ionic strength can enhance its dissolution by decreasing the activity coefficient of reacting aqueous species, and thus can promote iodine release from apatite. Non-neutral pH conditions clearly enhance the dissolution rate and can often lead to precipitations of secondary phases, such as chervetite and hydroxylvanadinite. The secondary phase precipitation at the surfaces hinders the dissolution rate because it reduces the available reacting surface area. However, the overall iodine release rates in both basic and acidic solutions are exponentially higher than those in the near-neutral pH conditions, especially in deionized water. These impacts of solution chemistry on dissolution add complexities to the current understanding of dissolution kinetics which is based on leaching experiments conducted solely in deionized water. This study suggests that, compared to fresh water with low ion concentrations, high concentrations of aqueous species commonly found in underground brines is detrimental to the chemical durability of apatite waste form in a geological repository. For this specific waste form, maintaining neutral pH and low ion content in aqueous solutions are critical to ensure the disposal safety of radioactive iodine. Since iodine is one of the most challenging radionuclides to

immobilize, building a comprehensive theoretical framework of iodine immobilization can significantly advance the research in nuclear waste disposal safety.

Conflicts of interest

There are no conflicts to declare.

Acknowledgements

References

1   Intergovernmental Panel on Climate Change and O. Edenhofer, Eds., *Climate change 2014: mitigation of climate change: Working Group III contribution to the Fifth Assessment Report of the Intergovernmental Panel on Climate Change*, Cambridge University Press, New York, NY, 2014.

2   W. M. Alley and R. Alley, *Environ. Sci. Technol.*, 2014, 48, 2091–2096.

3   A. L. Nichols, M. Verpelli and D. L. Aldama, *Handbook of nuclear data for safeguards*, International Atomic Energy Agency, 2007.

4   M. I. Ojovan and W. E. Lee, in *An Introduction to Nuclear Waste Immobilisation (Second Edition)*, eds. M. I. Ojovan and W. E. Lee, Elsevier, Oxford, 2014, pp. 107–115.

5   L. Aimoz, E. Wieland, C. Taviot-Guého, R. Dähn, M. Vespa and S. V. Churakov, *Environ. Sci. Technol.*, 2012, 46, 3874–3881.

6   W. Um, R. J. Serne and K. M. Krupka, *Water Res.*, 2004, 38, 2009–2016.

7   P. J. Coughtrey and M. C. Thorne, *Radionuclide distribution and transport in terrestrial and aquatic ecosystems. A critical review of data*, 1983, vol. 1.

8   D. C. Whitehead, *Environ. Int.*, 1984, 10, 321–339.

9   K. A. Schwehr, P. H. Santschi, D. I. Kaplan, C. M. Yeager and R. Brinkmeyer, *Environ. Sci. Technol.*, 2009, 43, 7258–7264.

10   Y. S. Shimamoto, Y. Takahashi and Y. Terada, *Environ. Sci. Technol.*, 2011, 45, 2086–2092.

11   R. Fuge and C. C. Johnson, *Appl. Geochem.*, 2015, 63, 282–302.

12   L. Patrick, *Altern. Med. Rev.*, 2008, 13, 116–127.

13   F. Audubert, J. Carpena, J. L. Lacout and F. Tetard, *Solid State Ion.*, 1997, 95, 113–119.

14   T. J. Garino, T. M. Nenoff, J. L. Krumhansl and D. X. Rademacher, *J. Am. Ceram. Soc.*, 2011, 94, 2412–2419.

15   J. L. Krumhansl and T. M. Nenoff, *Applied Geochemistry*, 2011, 26, 57–64.

16   D. F. Sava, T. J. Garino and T. M. Nenoff, *Ind. Eng. Chem. Res.*, 2012, 51, 614–620.

17   D. F. Sava, M. A. Rodriguez, K. W. Chapman, P. J. Chupas, J. A. Greathouse, P. S. Crozier and T. M. Nenoff, *J. Am. Chem. Soc.*, 2011, 133, 12398–12401.

18   B. J. Riley, J. D. Vienna, D. M. Strachan, J. S. McCloy and J. L. Jerden, *J. Nucl. Mater.*, 2016, 470, 307–326.

19   G. S. Frankel, J. D. Vienna, J. Lian, J. R. Scully, S. Gin, J. V. Ryan, J. Wang, S. H. Kim, W. Windl and J. Du, *npj Mater. Degrad.*, 2018, 2, 15.

20   P. Faucon, F. Adenot, J. F. Jacquinot, J. C. Petit, R. Cabrillac and M. Jorda, *Cem. Concr. Res.*, 1998, 28, 847–857.

21   G. S. Frankel, J. Vienna and J. Lian, *npj Mater. Degrad.*, 2017, 1, 5.

22   N. A. Chapman, I. G. McKinley and J. a. T. Smellie, *The potential of natural analogues in assessing systems for deep disposal of high-level radioactive waste*, Eidgenoessisches Inst. fuer Reaktorforschung, Sweden, 1984.

23   H. Kato, O. Kato and H. Tanabe, , DOI:10.11484/JAERI-Conf-2002-004.

24   T. Lemesle, F. O. Méar, L. Campayo, O. Pinet, B. Revel and L. Montagne, *J. Hazard. Mater.*, 2014, 264, 117–126.

25   T. Yao, F. Lu, H. Sun, J. Wang, R. C. Ewing and J. Lian, *J. Am. Ceram. Soc.*, 2014, 97, 2409–2412.

26   E. Maddrell, A. Gandy and M. Stennett, *Journal of Nuclear Materials*, 2014, 449, 168–172.

27	S. Chong, J. A. Peterson, B. J. Riley, D. Tabada, D. Wall, C. L. Corkhill and J. S. McCloy, *J. Nucl. Mater.*, 2018, 504, 109–121.

28	S. Le Gallet, L. Campayo, E. Courtois, S. Hoffmann, Yu. Grin, F. Bernard and F. Bart, *J. Nucl. Mater.*, 2010, 400, 251–256.

29	Z. Zhang, A. Heath, K. T. Valsaraj, W. L. Ebert, T. Yao, J. Lian and J. Wang, *RSC Adv.*, 2018, 8, 3951–3957.

30	F. Gauthier-Lafaye, *C. R. Phys.*, 2002, 3, 839–849.

31	M. Uno, M. Shinohara, K. Kurosaki and S. Yamanaka, *J. Nucl. Mater.*, 2001, 294, 119–122.

32	National Research Council, *scho*, 2011.

33	C. Guy, F. Audubert, J.-E. Lartigue, C. Latrille, T. Advocat and C. Fillet, *C. R. Phys.*, 2002, 3, 827–837.

34	M. Zhang, E. R. Maddrell, P. K. Abraitis and E. K. H. Salje, *Mater. Sci. Eng. B*, 2007, 137, 149–155.

35	A. Coulon, A. Grandjean, D. Laurencin, P. Jollivet, S. Rossignol and L. Campayo, *J. Nucl. Mater.*, 2017, 484, 324–331.

36	*ASTM C1220-17, Standard Test Method for Static Leaching of Monolithic Waste Forms for Disposal of Radioactive Waste*, ASTM International, West Conshohocken, PA, 2017.

37	Z. Zhang, W. L. Ebert, T. Yao, J. Lian, K. T. Valsaraj and J. Wang, *ACS Earth Space Chem.*, 2019, 3, 452-462 .

38	Y. Zhu, X. Zhang, Y. Chen, Q. Xie, J. Lan, M. Qian and N. He, *Chem. Geol.*, 2009, 268, 89–96.

39	S. Cazalbou, D. Eichert, X. Ranz, C. Drouet, C. Combes, M. F. Harmand and C. Rey, *J. Mater. Sci. Mater. Med.*, 2005, 16, 405–409.

40	J. Brenan, *Chem. Geol.*, 1993, 110, 195–210.

41	S. V. Dorozhkin, *Prog. Cryst. Growth Charact.*, 2002, 44, 45–61.

42	V. Petříček, M. Dušek and L. Palatinus, *Z. Kristallogr. Cryst. Mater.*, 2014, 229, 345–352.

43	F. Audubert, J.-M. Savariault and J.-L. Lacout, *Acta Crystallogr. C*, 1999, 55, 271–273.

44	A. Ślósarczyk, Z. Paszkiewicz and C. Paluszkiewicz, *J. Mol. Struct.*, 2005, 744–747, 657–661.

45	J. C. Merry, I. R. Gibson, S. M. Best and W. Bonfield, *J. Mater. Sci. Mater. Med.*, 1998, 9, 779–783.

46	H. K. Roobottom, H. D. B. Jenkins, J. Passmore and L. Glasser, *J. Chem. Educ.*, 1999, 76, 1570.

47	M. W. Guidry and F. T. Mackenzie, *Geochim. Cosmochim. Acta*, 2003, 67, 2949–2963.

48	C. Cao, S. Chong, L. Thirion, J. C. Mauro, J. S. McCloy and A. Goel, *J. Mater. Chem. C*, 2017, 5, 14331–14342.

49	L. Campayo, F. Audubert, J.-E. Lartigue, E. Courtois-Manara, S. L. Gallet, F. Bernard, T. Lemesle, F. O. Mear, L. Montagne, A. Coulon, D. Laurencin, A. Grandjean and S. Rossignol, *Mater. Res. Soc. Symp. Proc.*, 2015, 1744, 15–20.

50	R. Zapanta-Legeros, *Nature*, 1965, 206, 403.

51	T. J. White and Z. L. Dong, *Acta Cryst. B*, 2003, 59, 1–16.

52	M. E. Fleet and X. Liu, *Biomaterials*, 2007, 28, 916–926.

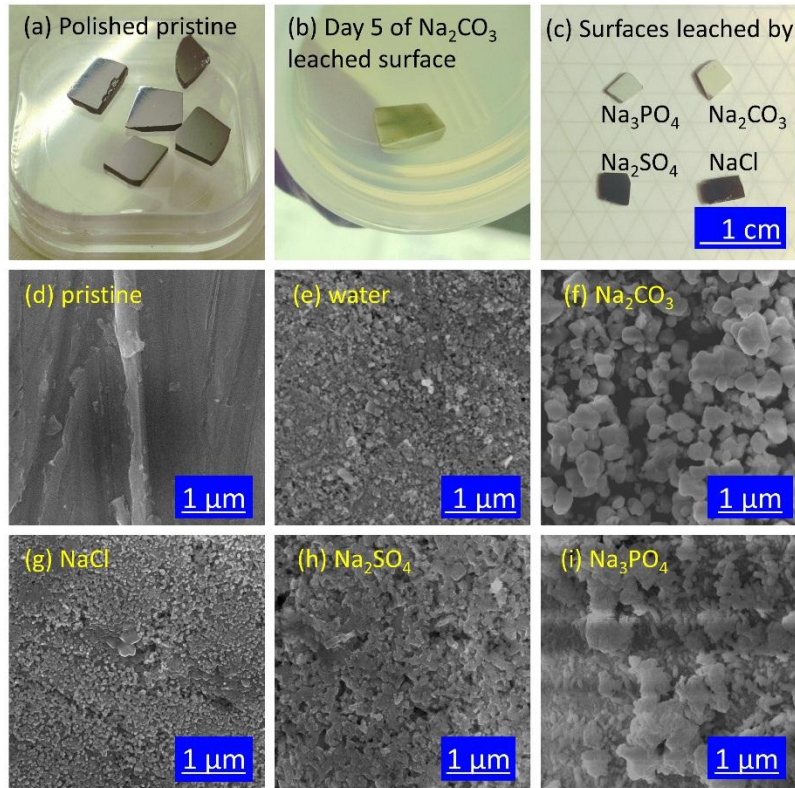53	E. Landi, A. Tampieri, G. Celotti, L. Vichi and M. Sandri, *Biomaterials*, 2004, 25, 1763–1770.
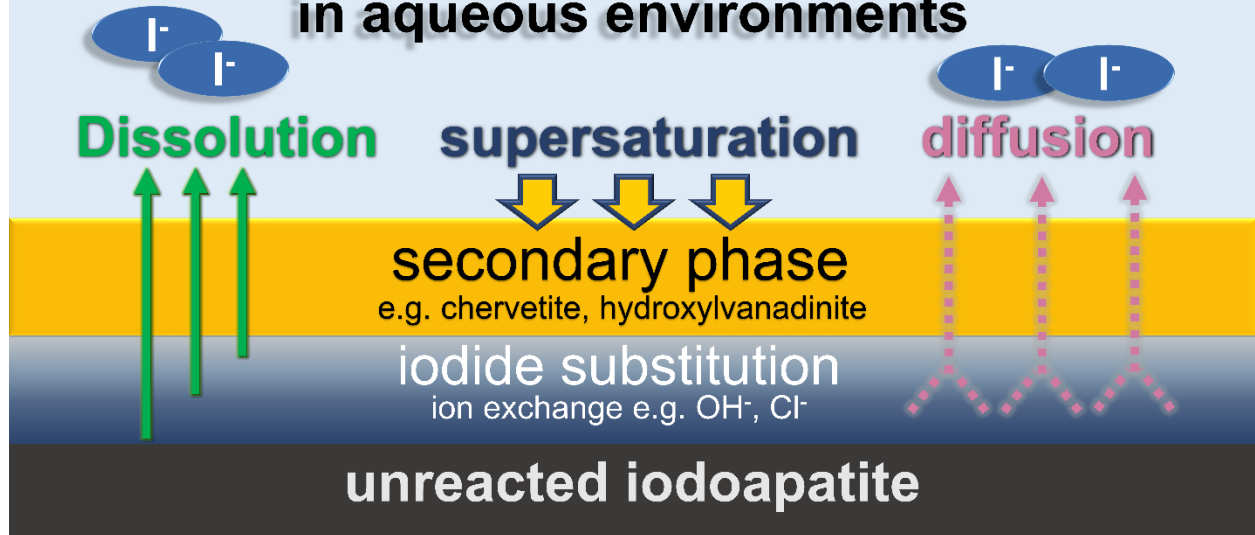
Figure 1.(a) Polished pristine iodoapatite samples before test, (b) iodoapatite leached surface during the 5th replacement of Na₂CO₃ solution, (c) surface leached by at the end of 14-day leaching tests, SEM images of (a) a polished pristine iodoapatite and the samples leached by (b) deionized water, (c) 0.1 mol/L Na₂CO₃, (d) 0.1 mol/L NaCl, (e) 0.1 mol/L Na₂SO₄, and (f) 0.1 mol/L Na₃PO₄.

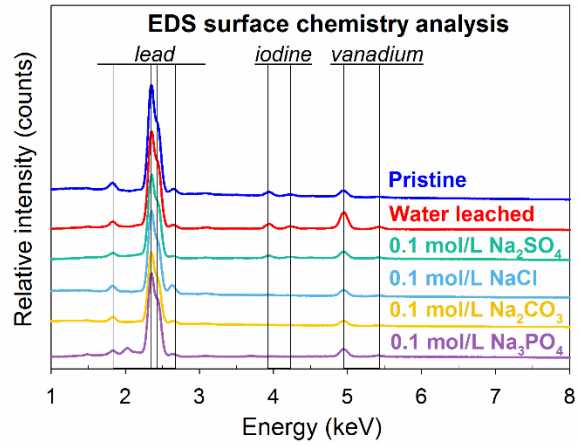Figure 2. EDS spectra of a pristine iodoapatite and the samples leached by deionized water, 0.1 mol/L NaCl, 0.1 mol/L Na_2CO_3, 0.1 mol/L Na_3PO_4, and 0.1 mol/L Na_2SO_4 solutions.
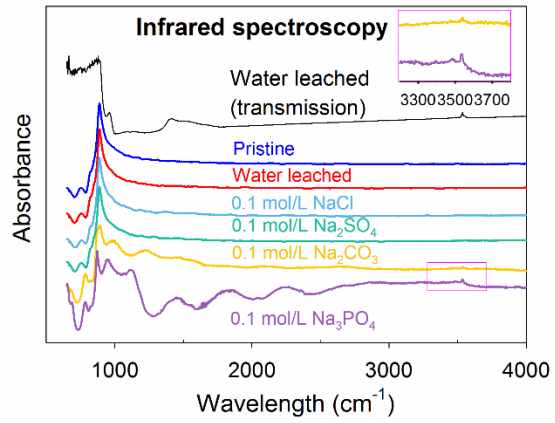
Figure 3. Infrared spectroscopy of pristine iodoapatite and leached samples by deionized water, NaCl, Na_2SO_4, Na_2CO_3, and Na_3PO_4 solutions.
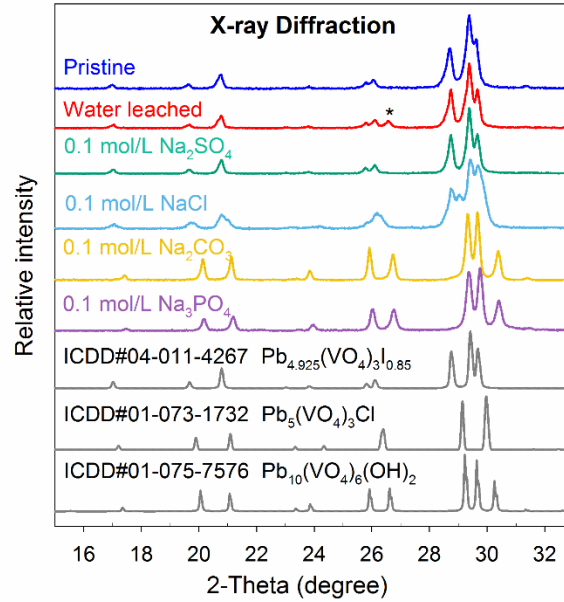
Figure 4. XRD patterns of a pristine iodoapatite and the samples leached by deionized water, 0.1 mol/L Na_2SO_4, 0.1 mol/L NaCl, 0.1 mol/L Na_2CO_3, and 0.1 mol/L Na_3PO_4. In addition, standard XRD spectra of iodoapatite, vanadinite, and hydroxylvanadinite are listed for comparison.
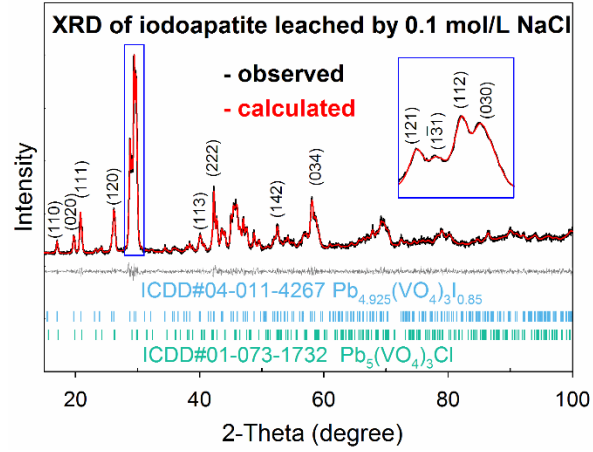
Figure 5. XRD phase analysis of the iodoapatite sample surface leached by 0.1 mol/L NaCl solution. Two phases were identified: iodoapatite and vanadinite.
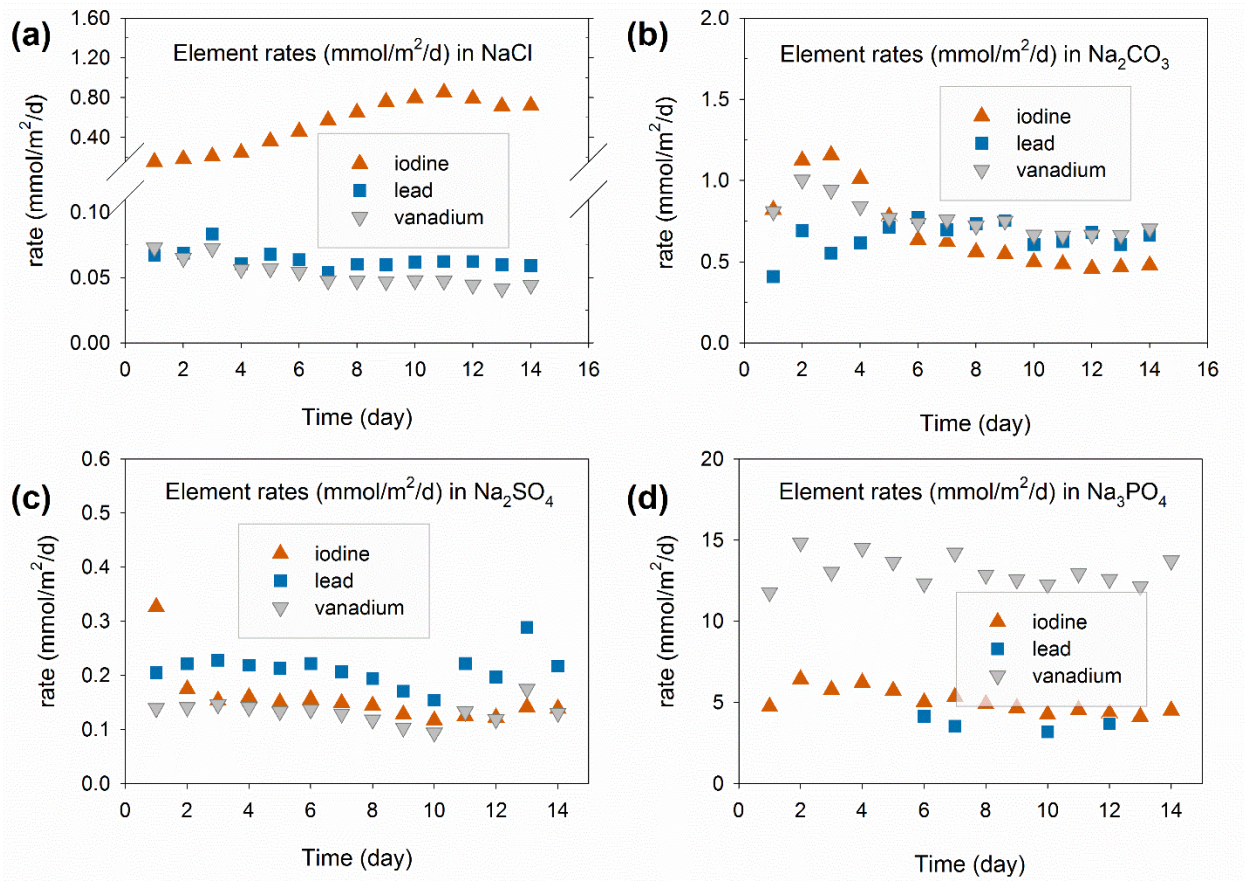
Figure 6. Solution analysis of collected leachates from 14 days semi-dynamic leach tests on iodoapatite samples in (a) 0.1 mol/L NaCl, (b) 0.1 mol/L Na_2CO_3, (c) 0.1 mol/L Na_2SO_4, and (d) 0.1 mol/L Na_3PO_4.
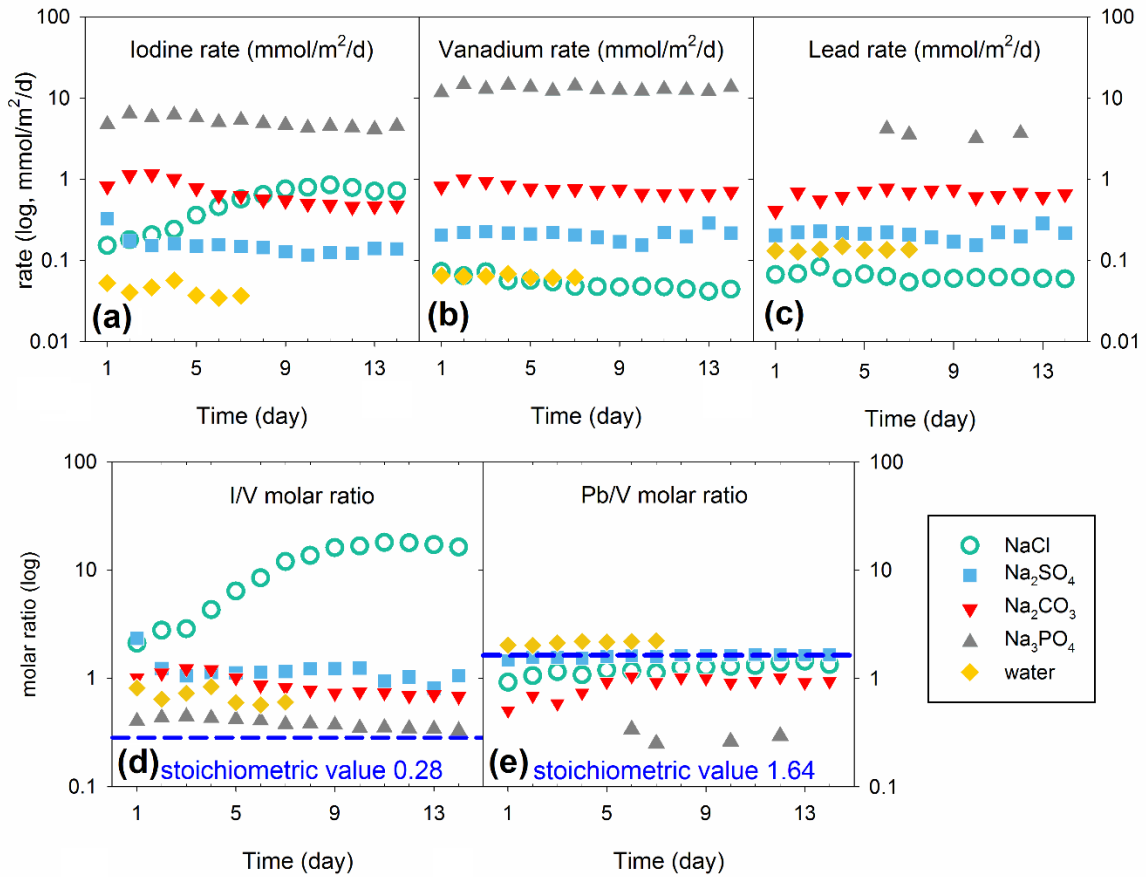
Figure 7. Comparison of element release rate of iodine (a), vanadium (b), and lead (c) in the leachate solutions from different leach tests. Molar ratios of Pb/V (d) and I/V (e) in leachate solutions from leach tests in NaCl, Na_2SO_4, Na_2CO_3, Na_3PO_4, and deionized water.
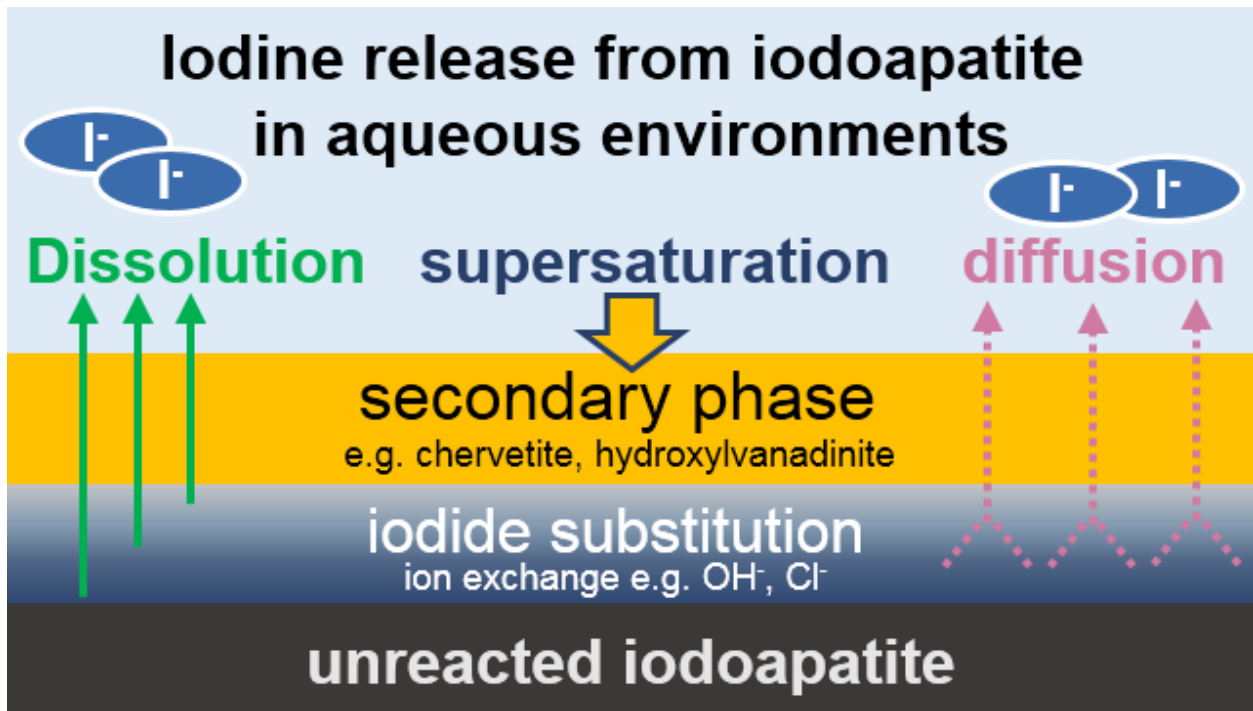
Figure 8. Schematic diagram illustrates major processes that control the iodine release from iodoapatite in aqueous environments

Table. 1 Crystallographic parameters based on the XRD refinements by Le Bail algorithm.

Leach test condition	Refined parameters				
	a, b (a=b, Å)	c (Å)	GoF	R_p (%)	R_{wp} (%)
Pristine	10.4420 (3)	7.4756 (3)	1.32	5.16	6.53
Water	10.4325 (3)	7.4864 (3)	1.63	6.04	7.73
0.1 mol/L Na₂SO₄	10.4336 (2)	7.4837 (2)	1.39	4.60	5.93
0.1 mol/L Na₂CO₃	10.1923 (2)	7.4656 (2)	1.65	4.85	6.44
0.1 mol/L Na₃PO₄	10.1984 (2)	7.4449 (2)	1.43	4.74	6.23
0.1 mol/L NaCl (2 phases)	10.4443 (6)	7.4796 (5)	1.17	4.12	5.28
	10.3536 (8)	7.3735(8)			
Pb₄.₉₂₅(VO₄)₃I₀.₈₅ [ICDD#04-011-4267]	10.422	7.467	**Crystal system: hexagonal**		
Pb₅(VO₄)₃(OH) [ICDD#01-075-7576]	10.2242	7.4537	**Space group: P63/m #176;**		
Pb₅(VO₄)₃Cl [ICDD#01-073-1732]	10.31	7.34	**α=90° β=90° γ=120°**		

Table 2. Solution chemistry at equilibrium state calculated by Visual MINTEQ under 90 °C.

mol/L 90 °C	Deionized water	0.1 mol/L NaCl	0.1 mol/L Na$_2$SO$_4$	0.1 mol/L Na$_2$CO$_3$	0.1 mol/L Na$_3$PO$_4$
pH (unitless)	6.1	6.1	6.2	10.3	10.9
Ionic strength	2.04×10^{-6}	0.098	0.26	0.25	0.29
Major cation	**H$^+$**	**Na$^+$**	**Na$^+$**	**Na$^+$**	**Na$^+$**
Concentration	6.52×10^{-7}	0.098	0.18	0.18	0.22
Activity	6.51×10^{-7}	0.074	0.13	0.13	0.15
Activity coefficient	1.00	0.76	0.72	0.72	0.68
Major anion	**OH$^-$**	**Cl$^-$**	**SO$_4^{2-}$**	**CO$_3^{2-}$**	**PO$_4^{3-}$**
Concentration	8.72×10^{-7}	0.098	0.079	0.069	0.012
Activity	8.70×10^{-7}	0.074	0.02	0.017	0.00049
Activity coefficient	1.00	0.76	0.25	0.24	0.041